Bit-Error-Rate Performance of an Underwater Wireless Optical Link Under Misalignment and Turbulence Effects

Ikenna Chinazaekpere Ijeh, Mohammad Ali Khalighi, Mohammed Elamassie, Steve Hranilovic, Murat Uysal

Bit-Error-Rate Performance of an Underwater Wireless Optical Link Under Misalignment and Turbulence Effects

1st Ikenna Chinazaekpere Ijeh
Department of Electrical/Electronic Engineering
Alex Ekwueme Federal University Ndufu-Alike Ikwo
Ebonyi State, Nigeria
Ikenna.Ijeh@funai.edu.ng

2nd Mohammad Ali Khalighi
Aix Marseille University, CNRS
Centrale Marseille, Institut Fresnel
Marseille, France
Ali.Khalighi@fresnel.fr

3rd Mohammed Elamassie
Department of Electrical & Electronics Engineering
Özyeğin University
Istanbul, Turkey
mohammed.elamassie@ozu.edu.tr

4th Steve Hranilovic
Department of Electrical & Computer Engineering
McMaster University
Hamilton, ON, Canada
hranilovic@mcmaster.ca

5th Murat Uysal
Department of Electrical & Electronics Engineering
Özyeğin University
Istanbul, Turkey
murat.uysal@ozyegin.edu.tr

***Abstract*—Underwater wireless optical communication (UWOC) links are highly susceptible to the degrading effects of oceanic turbulence and beam misalignment. In this paper, considering a silicon photo-multiplier at the receiver, we evaluate the link average bit-error rate (BER) performance, where an analytical expression is derived for its calculation, validated further by means of numerical simulations. We further investigate the impact of different system parameters on the link average BER.**

***Index Terms*—Underwater wireless optical communications, oceanic turbulence, pointing errors, silicon photo-multiplier**

I. Introduction

By enabling high rate, low latency, and energy-efficient data transmission, the underwater wireless optical communication (UWOC) technology has recently attracted considerable attention in diverse underwater applications [1]. However, implementing such links under practical conditions comes along with a number of challenges. In fact, in addition to the high signal attenuation in water, in particular in relatively high-turbidity waters, transmitter (Tx) - receiver (Rx) misalignment and oceanic turbulence can seriously impact the performance of UWOC links.

To deal with the relatively high channel loss, the use of ultra-sensitive photodetectors such as silicon photo-multipliers (SiPMs) has received particular attention recently [2]. On the other hand, beam misalignment, and consequently, the pointing errors (PEs) between the Tx and the Rx can be due to the instability and/or random movement of the platforms, which could be buoys, autonomous underwater vehicles (AUVs), etc. These can be as a result of sea surface roughness, underwater currents, accuracy of the mechanical stability system, for instance. The oceanic turbulence, in turn, can arise from fluctuations in the water refractive index due to variations in pressure, temperature and salinity, or otherwise, oceanic currents [3].

A few previous works considered channel modeling and performance study of UWOC systems subject to PEs and turbulence [3]–[8]. For instance, [4] studied the impact of wind speed on a buoy-based vertical link. A geometric loss model was proposed in [5] to investigate the impact of angular PEs on the link bit-error-rate (BER) performance. Also, the impact of Tx-Rx parameter optimization on minimizing the effect of PEs was studied in [6]. An experimentally verified statistical model for turbulence induced by air bubbles and temperature gradient was proposed in [7]. Also, for a vertical turbulent link, [3] proposed a close-to-reality mathematical model that took into account temperature and salinity variations with depth.

This work focuses on the impact of PEs and oceanic turbulence on the average BER performance of a vertical UWOC link between a buoy and an AUV. While taking into account the effect of solar radiations, we provide approximate and analytical BER expressions for a laser-based Tx and an SiPM-based Rx, which are validated through simulations. Based on this, we study the impact of Tx/Rx parameters on the link performance.

We present in Section II the channel and system model, and then provide in Section III the derivation of the BER approximate and analytical expression. Numerical results for link performance study are presented in Section IV, and main conclusions are provided in Section V.

This work was partly supported by Alex Ekwueme Federal University Ndufu-Alike (AE-FUNAI) in partnership with the Embassy of France in Nigeria and Campus France. It was also based upon work from European Union's Horizon 2020 COST Action CA19111 NEWFOCUS (European network on future generation optical wireless communication technologies).

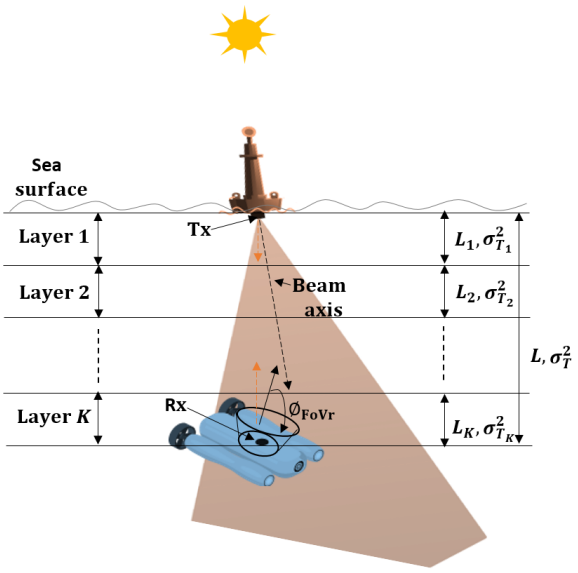

Fig. 1. Buoy-AUV illustration of the considered vertical UWOC link.

II. Channel and System Models

Fig. 1 shows an illustration of the considered vertical UWOC link of range (i.e. operational depth) L. The channel attenuation coefficient is considered as $h = h_c\, h_t\, h_p$, where h_c, h_t and h_p represent the propagation loss, turbulence, and PEs, respectively:

$$h = \underbrace{\exp(-L\, c_{\rm e})}_{h_c}\, \underbrace{\exp\left(T\right)}_{h_t}\, \underbrace{\exp\left(-2r_p^2/w_{Leq}^2\right) A_0}_{h_p}. \tag{1}$$

Here, $c_{\rm e}$ denotes the beam extinction coefficient [9], and T is the log-amplitude coefficient of turbulence that follows a Gaussian distribution with mean μ_T and variance σ_T^2 [10]. Also, r_p is the radial displacement of the transmitted beam spot at L from the center of the Rx lens. The beam spot has a beam width w_L with an equivalent parameter $w_{Leq} = \sqrt{w_L^2 \frac{\sqrt{\pi}\text{erf}(\nu)}{2\nu \exp(-\nu^2)}}$, where $\nu = (D_r\sqrt{\pi})/(2\sqrt{2}w_L)$ for a Rx lens diameter of D_r and erf$(\cdot)$ is the error function. Lastly, $A_0 = (\text{erf}(\nu))^2$ is the maximum fraction of received power at $r_p = 0$ [11].

For the signal transmission, we consider the non-return to zero (NRZ) on-off keying (OOK) modulation. We denote the transmitted OOK signal by s_i, which takes two intensity values of P_{Tx_0} for $i = 0$ and P_{Tx_1} for $i = 1$, related through the extinction ratio $\xi = P_{\text{Tx}_0}/P_{\text{Tx}_1}$.

At the Rx, the captured signal intensity generates a photo-current I_i at the SiPM output, expressed as:

$$I_i = \underbrace{I_{s,i} + I_d + I_b}_{\breve{I}_i} + n_{s_i}, \tag{2}$$

where $I_{s,i} = \mathcal{R}_{\rm e}\, s_i\, h$ represents the useful OOK signal with $\mathcal{R}_{\rm e}$ the SiPM responsivity [12], I_d is the dark current, I_b is due to the background radiations, and n_{s_i} is the Rx noise, including shot, dark current, and background noises. Denoting the downwelling spectral irradiance of the solar noise by $E_{\text{sun}}(\lambda, L)$, we have [8], [13]:

$$I_b = \mathcal{R}_{\rm e}\, \frac{E_{\text{sun}}(\lambda, 0)\, e^{-(L\, K_{\rm d})}}{E_{\text{sun}}(\lambda, L)}\, \pi \phi_{\text{FoVr}}^2\, T_w\, T_f\, B_o\, (\pi\, D_r^2/4). \tag{3}$$

TABLE I
Variables in (3) and (5)

Notation	Definition
$E_{\text{sun}}(\lambda, 0)$	Solar irradiance at the sea surface (i.e., at $L = 0$)
λ	Wavelength
$K_{\rm d}$	Diffuse attenuation coefficient
ϕ_{FoVr}	Rx field-of-view (FoV)
T_w	Water transmittance
T_f	Optical filter transmittance
B_o	Optical filter bandwidth
$n_{s_k} = 2\, e\, G\, F\, B_e$	Rx noise constant
e	Electron charge
G	SiPM gain
F	PD excess noise factor
B_e	LPF bandwidth
$K_{\rm Z}$	Boltzmann constant
T_e	Rx equivalent temperature in Kelvin

From (2), I_i passes through a trans-impedance amplifier (TIA) with load resistance $R_{\rm L}$, followed by a low-pass filter (LPF). Denoting the thermal noise by n_{th}, the LPF output r_i is:

$$r_i = R_{\rm L}\, I_i + n_{\text{th}} = R_{\rm L}\, \breve{I}_i + R_{\rm L}\, n_{s_i} + n_{\text{th}}. \tag{4}$$

Denoting by $\sigma_{\text{sh},i}^2$, $\sigma_{\rm d}^2$, $\sigma_{\rm b}^2$, and σ_{th}^2 the variances of the shot, dark, background, and thermal noises, respectively, the total noise variance is:

$$\sigma_{n_i}^2 = R_{\rm L}^2 \underbrace{\left(\sigma_{\text{sh},i}^2 + \sigma_{\rm d}^2 + \sigma_{\rm b}^2\right)}_{n_{s_k}(I_{s,i} + I_d + I_b)} + \underbrace{\sigma_{\text{th}}^2}_{4\, K_{\rm Z}\, T_e\, B_e\, R_{\rm L}}. \tag{5}$$

III. Bit-Error-Rate Performance

Given the signal-dependent noise for the SiPM-based Rx, the following equation gives the instantaneous link BER $P_e(e|h)$ [14]:

$$P_e(e|h) = \frac{1}{4}\text{erfc}\left(\frac{\gamma_{\text{th}} - R_{\rm L}\, \breve{I}_0}{\sqrt{2\, \sigma_{n_0}^2}}\right) + \frac{1}{4}\text{erfc}\left(\frac{R_{\rm L}\, \breve{I}_1 - \gamma_{\text{th}}}{\sqrt{2\, \sigma_{n_1}^2}}\right), \tag{6}$$

where γ_{th} denotes the optimal demodulation threshold (see [6] for details) and erfc$(\cdot)$ is the complementary error function. Given the very large SiPM gain, we reasonably assume that the Rx noise is dominated by shot noise [6]. Hence, assuming a relatively large OOK extinction ratio ξ, we have $\breve{I}_0 \approx \xi\, \breve{I}_1$ and $\sigma_{n_0}^2 \approx \xi\, \sigma_{n_1}^2$. Then, γ_{th} can be simplified as $\gamma_{\text{th}} \approx R_{\rm L}\, I_{s,0}\, \sqrt{1/\xi}$. As a result,

$$P_e(e|h) \approx \frac{1}{2}\text{erfc}\left(\frac{R_{\rm L}\, I_{s,0}\, \sqrt{1/\xi} - R_{\rm L}\, I_{s,0}}{\sqrt{2\, \sigma_{n_0}^2}}\right). \tag{7}$$

Lets define for notation simplicity $\omega = R_{\rm L}\, \mathcal{R}_{\rm e}\, P_{\text{Tx}_0}$, $\alpha = 2\, e\, G\, F\, B_e\, R_{\rm L}\, \omega$, and $\beta = R_{\rm L}^2\, \sigma_{\rm d}^2 + R_{\rm L}^2\, \sigma_{\rm b}^2 + \sigma_{\text{th}}^2$. Then, (7) can be re-written as:

$$P_e(e|h) = \frac{1}{2}\text{erfc}\left(\frac{\omega\, h\, \left(\sqrt{1/\xi} - 1\right)}{\sqrt{2\, \alpha\, h + 2\, \beta}}\right). \tag{8}$$

The average BER is given by:

$$P_e = \int_0^\infty P_e(e|h)\, f_h(h) dh, \tag{9}$$

where $f_h(h)$ is the probability density function (PDF) of $h = h_c\, h_t\, h_p$ and can be expressed as:

$$f_h(h) = \int f_{h_t}(h_t)\ f_{h|h_t}(h|h_t)\ dh_t, \tag{10}$$

where

$$f_{h_t}(h_t) = \frac{1}{h_t\sqrt{2\pi\sigma_T^2}} \exp\left(-\frac{\left(\ln(h_t) - \mu_T\right)^2}{2\sigma_T^2}\right), \tag{11}$$

$$f_{h|h_t}(h|h_t) = \frac{1}{h_c\, h_t} f_{h_p}\left(\frac{h}{h_c\, h_t}\right). \tag{12}$$

Here μ_T and σ_T^2 are the mean and variance of T for the entire cascaded layers of the channel. Ocean waters are arranged in the form of layers where the densest water is below the less dense water [15]. This is due to the fact that the changes of both temperature and salinity are not smooth with depth but rather they change in a stepwise manner where gradient layers with a thickness that varies, typically, between few meters to tens of meters are separated by strong gradient sheets with thickness in the order of centimetres [16]–[20]. For a total of K layers, negligible change is assumed in the mean μ_{T_k} and variance $\sigma_{T_\mathrm{k}}^2$ of a k^{th} layer of thickness L_k, but the changes are distinct across layers [3]. Considering the induced-fading through the layers follow an independent and non-identical Gaussian distribution, $\mu_T = \sum_{k=1}^{K} 2\mu_{T_\mathrm{k}}$ and $\sigma_T^2 = \sum_{k=1}^{K} 4\sigma_{T_\mathrm{k}}^2$. Note that to normalize the fading coefficient, we set $\mu_{T_\mathrm{k}} = -\sigma_{T_\mathrm{k}}^2$, and $\sigma_{T_\mathrm{k}}^2 = 0.25\ln(1+\sigma_{I_\mathrm{k}}^2)$, where $\sigma_{I_\mathrm{k}}^2$ is the scintillation index with detailed computation approach in [3]. Since we consider a weak turbulence regime, $\sigma_{I_\mathrm{k}}^2 < 1$. Also, the PDF of h_p, $f_{h_p}(h_p)$ is given as [11]:

$$f_{h_p}(h_p) = \frac{\frac{w_{Leq}^2}{4\,\sigma_{r_p}^2}}{A_0^{\frac{w_{Leq}^2}{4\,\sigma_{r_p}^2}}}\, h_p^{\frac{w_{Leq}^2}{4\,\sigma_{r_p}^2}-1}, \tag{13}$$

where $\sigma_{r_p}^2$ denotes the jitter variance of r_p which is assumed to follow a Rayleigh distribution.

Considering $0 \le h \le A_0\, h_c\, h_t$, and after some mathematical manipulations, $f_h(h)$ in (10) can be expressed as:

$$f_h(h) = \frac{\left(A_0\, h_c\right)^{-\frac{w_{Leq}^2}{4\,\sigma_{r_p}^2}}}{\sqrt{\pi}}\, \frac{w_{Leq}^2}{4\,\sigma_{r_p}^2}\, h^{\frac{w_{Leq}^2}{4\,\sigma_{r_p}^2}-1} \int_{h/A_0\, h_c}^{\infty} h_t^{-\frac{w_{Leq}^2}{4\,\sigma_{r_p}^2}-1}\, \frac{1}{\sqrt{2\sigma_T^2}} \exp\left(-\frac{\left(\ln(h_t) - \mu_T\right)^2}{2\sigma_T^2}\right) dh_t. \tag{14}$$

Now using (14), (8) and after some mathematical derivations presented in Appendix A, P_e in (9) is calculated using the expression:

$$P_e \approx \left(A_0\, h_c\right)^{-\frac{w_{Leq}^2}{4\,\sigma_{r_p}^2}}\, \frac{w_{Leq}^2}{16\,\sigma_{r_p}^2} \exp\left(-\mu_T \frac{w_{Leq}^2}{4\,\sigma_{r_p}^2}\right) \exp\left(\sigma_T^2 \frac{w_{Leq}^4}{32\,\sigma_{r_p}^4}\right) \int_0^\infty h^{\frac{w_{Leq}^2}{4\,\sigma_{r_p}^2}-1} \operatorname{erfc}\left(\frac{\omega\left(\sqrt{\frac{1}{\xi}}-1\right)}{\sqrt{2\,\alpha\, h + 2\,\beta}}\, h\right) \operatorname{erfc}\left(\frac{\ln(h)}{\sqrt{2\,\sigma_T^2}} - \frac{\ln(A_0\, h_c) + \mu_T}{\sqrt{2\,\sigma_T^2}} + \sqrt{2\,\sigma_T^2}\, \frac{w_{Leq}^2}{8\,\sigma_{r_p}^2}\right) dh. \tag{15}$$

TABLE II
SIMULATION PARAMETERS

Parameter	Value
LD wavelength λ	450 nm
LD peak transmit power P_{Tx_1}	100 mW
OOK extinction ratio ξ	0.4
Bit rate R_b	1 Mbps
Beam extinction coefficient c_e	$\approx 0.151\,\mathrm{m}^{-1}$
Diffuse attenuation coefficient K_d	$\approx 0.08\,\mathrm{m}^{-1}$
Water transmittance T_w	≈ 0.97
Optical filter transmittance T_f	1
Optical filter bandwidth B_o	2 nm
LPF bandwidth B_e	$\approx R_\mathrm{b}/2$
Rx lens diameter D_r	75 mm
SiPM gain G	10^6
SiPM responsivity $\mathcal{R}_\mathrm{e}$	7.58×10^{17} A/W
SiPM dark current I_d	$1.10\,\mu$A
SiPM excess noise factor F	1.1
TIA load resistance R_L	1 kΩ

IV. NUMERICAL RESULTS

In this section, considering operations in clear waters using a laser diode (LD) of wavelength $\lambda = 450$ nm at the Tx, we present numerical results to study the impact of turbulence, PEs, and solar radiations on the link BER performance. In the cascaded-layer turbulence model, layers of thickness of 30 m are considered (in fact, the study in [21] showed that there are relatively insignificant changes in temperature and salinity of seawater within a range of 30 m thickness). The other simulation parameters are given in Table II. In the numerical results, we present the BER obtained using the analytical expression of (15) and based on simulations of 10^8 channel realizations of (6) and its approximation (7). The latter is considered to verify the validity of our assumptions in realizing (15).

Fig. 2 presents the BER plots versus the data rate R_b for three link ranges L, each corresponding to a specific turbulence parameter σ_T^2. Note, we do not take into account the limited bandwidth of the SiPM here [2]. Also, PEs and solar noise are neglected in the presented results. Given the layer thickness of 30 m in the cascaded turbulence model, the turbulence parameters for each layer in the case of $L = 120$ m are $\sigma_{T_1}^2 = 9.26\times10^{-2}$, $\sigma_{T_2}^2 = 8.32\times10^{-2}$, $\sigma_{T_3}^2 = 7.10\times10^{-2}$, and $\sigma_{T_4}^2 = 5.57\times10^{-2}$, computed from the profile of the Pacific Ocean at high latitudes with temperature and salinity ranges of $0\,^\circ - 8^\circ$C and $35.5 - 36.25$ PPT (Parts Per Thousand),

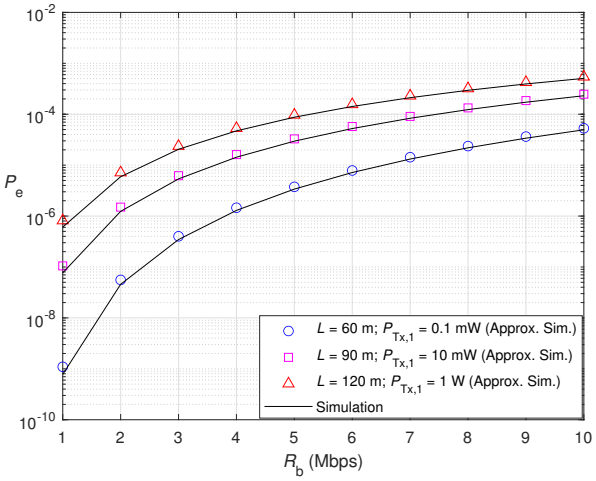

Fig. 2. Effect of data rate R_b and link range L on BER. $\phi_\text{FoVr} = 90°$, negligible PEs and solar noise.

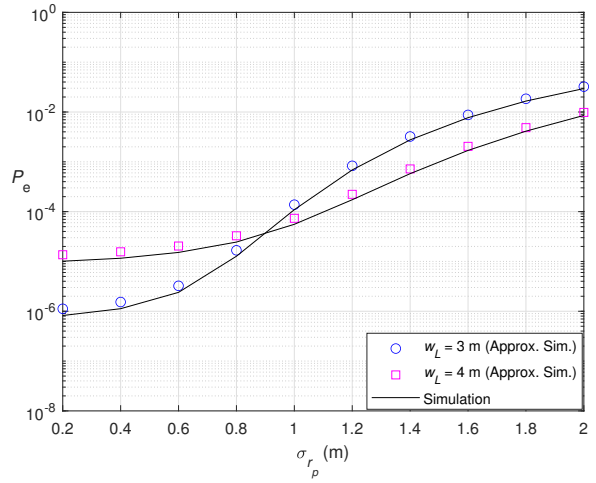

Fig. 3. Effect of jitter variance σ_{r_p} and beam width w_L on BER. ϕ_FoVr = 90°, $P_\text{Tx,1} = 100\,\text{mW}$, $L = 60\,\text{m}$, $\sigma_T^2 = 0.7032$, $R_\text{b} = 1\,\text{Mbps}$, negligible solar noise.

respectively [21][1]. Hence, for $L = 60$, 90 and 120 m, we have $\sigma_T^2 = 0.7032$, 0.9872, and 1.21, respectively. We have additionally adjusted the Tx peak optical power $P_\text{Tx,1}$ to 0.1 mW, 10 mW and 1 W, respectively.

First notice that the derived approximate BER expression [denoted as "Approx. Sim." and obtained using (7)] provides a quite tight upper-bound on the BER, very close to the simulation results [with the legend "Simulation"]. As expected, for a longer L, the turbulence strength increases, resulting in degraded BER and the requirement of a higher transmit power. It is further noticed that for a given L, the BER deteriorates with increase in R_b, which is due to the increase in the noise variance $\sigma_{n_i}^2$ (note, bandwidth of the LPF depends on R_b [23]).

[1]For computing the variance of log-amplitude coefficient in each layer, dissipation rate of mean-squared temperature and dissipation rate of turbulent kinetic energy per unit mass of fluid are assumed, respectively, as 1×10^{-3} K^2s^{-3} and 1×10^{-2} m^2s^{-3} (These are two important parameters of the spectrum model in [22]).

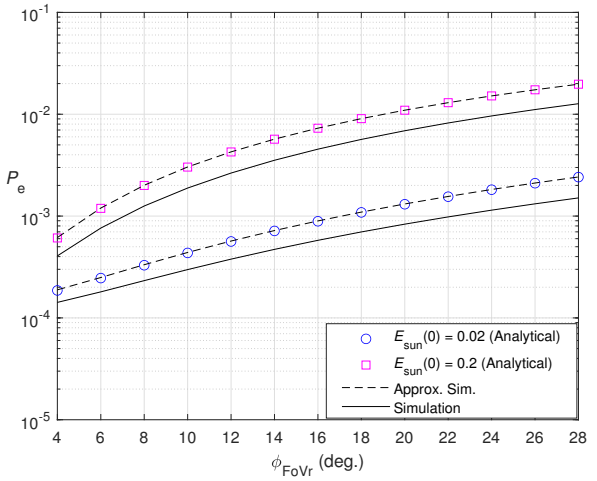

Fig. 4. Effect of Rx FoV ϕ_FoVr and $E_\text{sun}(0)$ on BER; $P_\text{Tx,1} = 100\,\text{mW}$, $L = 60\,\text{m}$, $\sigma_T^2 = 0.7032$, $R_\text{b} = 1\,\text{Mbps}$, $\sigma_{r_p} = 1\,\text{m}$, $w_L = 3\,\text{m}$.

For instance, assuming a target BER of 10^{-6}, R_b is limited to about 3, 2, and 1 Mbps, for link ranges of $L = 60$, 90 and 120 m, respectively.

To see the impact of PEs, we fix $L = 60\,\text{m}$, which corresponds to $\sigma_T^2 = 0.7032$, while still neglecting solar radiations. Fig. 3 shows the BER results as a function of the jitter variance σ_{r_p} for two beam widths of $w_L = 3$ and 4 m. As expected, as σ_{r_p} increases, the link performance deteriorates. For relatively small σ_{r_p}, i.e., smaller than $\sim 0.8\,\text{m}$, a narrower beam offers a better link performance due to a low geometric loss. However, as σ_{r_p} increases, i.e., for $\sigma_{r_p} \gtrsim 1\,\text{m}$, the impact of PEs is relaxed by choosing a wider beam.

Lastly, we study the link performance affected by turbulence and link misalignment while taking into account solar radiation. Considering $E_\text{sun}(\lambda, 0) = 0.02$ and $0.2\,\text{Wm}^{-2}\text{nm}^{-1}$, the impact of the Rx FoV ϕ_FoVr on the BER is shown in Fig. 4. Note that $E_\text{sun}(\lambda, 0) = 0.2\,\text{Wm}^{-2}\text{nm}^{-1}$ relates to $\lambda = 450\,\text{nm}$ when the Sun is at 60° with respect to its zenith over a hazy sky [9]. First we notice that the analytical and approximate BER results are less accurate to that of the simulations, this is due to the assumption of the negligible impact of solar noise in their derivations (compare the accuracy of results in Figs. 2 and 3, in the absence of solar noise). It can be seen that as ϕ_FoVr increases, the BER deteriorates, which is due to capturing more solar noise at the Rx for a larger FoV. In practice, the choice of ϕ_FoVr should trade-off the received solar noise and sensitivity to PEs as discussed in [8].

V. Conclusions

This work investigated the effect of oceanic turbulence, PEs and solar radiations on the BER performance of a vertical UWOC link. An analytical expression was derived for the average BER, which was validated through simulations. We examined the impact of different link parameters including range, the Tx beam divergence, and Rx FoV on the link performance. Specifically, the results showed the trade-off to make on the choice of the Tx beam divergence and Rx FoV, which impact PEs and captured solar radiations, respectively.

APPENDIX A
DERIVATION OF THE ANALYTICAL EXPRESSION FOR AVERAGE BER

To obtain the P_e expression in (15), we first express (9) using (14) and (8) as:

$$P_e = \frac{(A_0\, h_c)^{-\frac{w_{Leq}^2}{4\,\sigma_{r_p}^2}}}{\sqrt{\pi}}\, \frac{w_{Leq}^2}{4\,\sigma_{r_p}^2} \int_0^{\infty} h^{\frac{w_{Leq}^2}{4\,\sigma_{r_p}^2}-1}\, \frac{1}{2}\, \text{erfc}\left(\frac{\omega\, h\, \left(\sqrt{\frac{1}{\xi}}-1\right)}{\sqrt{2\,\alpha\, h + 2\,\beta}}\right) dh \int_{h/A_0\, h_c}^{\infty} h_t^{-\frac{w_{Leq}^2}{4\,\sigma_{r_p}^2}-1}\, \frac{1}{\sqrt{2\sigma_T^2}}\, \exp\left(-\frac{\left(\ln(h_t)-\mu_T\right)^2}{2\sigma_T^2}\right) dh_t. \tag{16}$$

Next, we carry out a variable change in (16), $X = (\ln(h_t) - \mu_T)/\sqrt{2\sigma_T^2}$, where we get:

$$P_e \approx \frac{(A_0\, h_c)^{-\frac{w_{Leq}^2}{4\,\sigma_{r_p}^2}}}{2\,\sqrt{\pi}}\, \frac{w_{Leq}^2}{4\,\sigma_{r_p}^2}\, \exp\left(-\mu_T \frac{w_{Leq}^2}{4\,\sigma_{r_p}^2}\right) \exp\left(\sigma_T^2 \frac{w_{Leq}^4}{32\,\sigma_{r_p}^4}\right) \int_0^{\infty} h^{\frac{w_{Leq}^2}{4\,\sigma_{r_p}^2}-1}\, \text{erfc}\left(\frac{\omega\, \left(\sqrt{\frac{1}{\xi}}-1\right)}{\sqrt{2\,\alpha\, h + 2\,\beta}}\, h\right) dh \int_{X_l}^{\infty} \exp\left(-X^2 - \sqrt{2\,\sigma_T^2}\, \frac{w_{Leq}^2}{4\,\sigma_{r_p}^2}\, X\right) dX, \tag{17}$$

where $X_l = (\ln(h) - \ln(A_0\, h_c) - \mu_T)/\sqrt{2\sigma_T^2}$. Using [24, Section 2.33, Eq.(1)], the second integral in (17) can be solved and re-arranged as follows:

$$P_e \approx (A_0\, h_c)^{-\frac{w_{Leq}^2}{4\,\sigma_{r_p}^2}}\, \frac{w_{Leq}^2}{16\,\sigma_{r_p}^2}\, \exp\left(-\mu_T \frac{w_{Leq}^2}{4\,\sigma_{r_p}^2}\right) \exp\left(\sigma_T^2 \frac{w_{Leq}^4}{32\,\sigma_{r_p}^4}\right) \int_0^{\infty} h^{\frac{w_{Leq}^2}{4\,\sigma_{r_p}^2}-1}\, \text{erfc}\left(\frac{\omega\, \left(\sqrt{\frac{1}{\xi}}-1\right)}{\sqrt{2\,\alpha\, h + 2\,\beta}}\, h\right) \text{erfc}\left(\frac{\ln(h)}{\sqrt{2\,\sigma_T^2}} - \frac{\ln(A_0\, h_c) + \mu_T}{\sqrt{2\,\sigma_T^2}} + \sqrt{2\,\sigma_T^2}\, \frac{w_{Leq}^2}{8\,\sigma_{r_p}^2}\right) dh. \tag{18}$$

REFERENCES

[1] M. A. Khalighi, C. J. Gabriel, L. M. Pessoa, and B. Silva, *Visible Light Communications: Theory and Applications*. CRC-Press, 2017, ch. Underwater Visible Light Communications, Channel Modeling and System Design, pp. 337–372.

[2] M. A. Khalighi, T. Hamza, S. Bourennane, P. Léon, and J. Opderbecke, "Underwater wireless optical communications using silicon photomultipliers," *IEEE Photon. J.*, vol. 9, no. 4, 2017.

[3] M. Elamassie and M. Uysal, "Vertical underwater visible light communication links: Channel modeling and performance analysis," *IEEE Trans. Commun.*, vol. 19, no. 10, pp. 6948–6959, 2020.

[4] Y. Dong, S. Tang, and X. Zhang, "Effect of random sea surface on downlink underwater wireless optical communications," *IEEE Commun. Lett.*, vol. 17, no. 11, pp. 2164–2167, Nov. 2013.

[5] R. Boluda-Ruiz, A. García-Zambrana, B. Castillo-Vázquez, and S. Hranilovic, "Impact of angular pointing error on BER performance of underwater optical wireless links," *Optics Express*, vol. 28, no. 23, pp. 34 606–34 622, Nov 2020.

[6] I. C. Ijeh, M. A. Khalighi, and S. Hranilovic, "Parameter optimization for an underwater optical wireless vertical link subject to link misalignments," *IEEE J. Ocean. Eng.*, vol. 46, no. 4, pp. 1424–1437, 2021.

[7] E. Zedini, H. M. Oubei, A. Kammoun, M. Hamdi, B. S. Ooi, and M.-S. Alouini, "Unified statistical channel model for turbulence-induced fading in underwater wireless optical communication systems," *IEEE Trans. Commun.*, vol. 67, no. 4, pp. 2893–2907, Apr. 2019.

[8] I. C. Ijeh, M. A. Khalighi, M. Elamassie, S. Hranilovic, and M. Uysal, "Outage probability analysis of a vertical underwater wireless optical link subject to oceanic turbulence and pointing errors," *IEEE/OSA J. Opt. Commun. Netw.*, vol. 14, no. 6, pp. 439–453, 2022.

[9] C. Mobley, E. Boss, and C. Roesler, "Ocean optics web book," http://www.oceanopticsbook.info/, last accessed: 16 Dec. 2021.

[10] M. V. Jamali, A. Mirani, A. Parsay, B. Abolhassani, P. Nabavi, A. Chizari, P. Khorramshahi, S. Abdollahramezani, and J. A. Salehi, "Statistical studies of fading in underwater wireless optical channels in the presence of air bubble, temperature, and salinity random variations," *IEEE Trans. Commun.*, vol. 66, no. 10, pp. 4706–4723, 2018.

[11] A. A. Farid and S. Hranilovic, "Outage capacity optimization for free-space optical links with pointing errors," *J. Lightw. Technol.*, vol. 25, no. 7, pp. 1702–1710, 2007.

[12] *Introduction to SiPM, Technical Note*. ON Semiconductor®, 2011 (Rev. 8.0, July 2021), available at https://www.onsemi.com/pub/Collateral/AND9770-D.PDF.

[13] T. Hamza, M. A. Khalighi, S. Bourennane, P. Léon, and J. Opderbecke, "Investigation of solar noise impact on the performance of underwater wireless optical communication links," *Optics Express*, vol. 24, no. 22, pp. 25 832–25 845, Oct. 2016.

[14] M. T. Dabiri, S. M. S. Sadough, and M. A. Khalighi, "FSO channel estimation for OOK modulation with APD receiver over atmospheric turbulence and pointing errors," *Optics Commun.*, vol. 402, pp. 577–584, 2017.

[15] R. Griffis and J. Howard, *Oceans and marine resources in a changing climate: a technical input to the 2013 national climate assessment*. Island Press, 2013.

[16] V. V. Nikishov and V. I. Nikishov, "Spectum of turbulence fluctuations of the sea-water refraction index," *Int. J. Fluid Mech. Res.*, vol. 27, no. 1, p. 8298, 2000.

[17] R. D. Muench, H. J. S. Fernando, and G. R. Stegen, "Temperature and salinity staircases in the northwestern weddell sea," *American Meteorological Society*, vol. 20, no. 2, pp. 295–306, Feb. 1990.

[18] G. Kullenberg, *Pollutant transfer and transport in the sea: Volume I*. CRC Press Boca Raton, Fla, 1982.

[19] G. D. Gilbert and R. C. Honey, "Optical turbulence in the sea," *Underwater Photo-Optical Instrumentation Applications*, vol. 0024, p. 4955, Jun. 1971.

[20] H. Stommel and K. N. Fedorov, "Small scale structure in temperature and salinity near timor and mindanao," *Tellus*, vol. 19, no. 2, p. 306325, 1967.

[21] M. Elamassie and M. Uysal, "Performance characterization of vertical underwater vlc links in the presence of turbulence," in *11th International Symposium on Communication Systems, Networks Digital Signal Processing (CSNDSP)*, 2018, pp. 1–6.

[22] M. Elamassie, M. Uysal, Y. Baykal, M. Abdallah, and K. Qaraqe, "Effect of eddy diffusivity ratio on underwater optical scintillation index," *J. Opt. Soc. Am. A*, vol. 34, no. 11, pp. 1969–1973, 2017.

[23] F. Xu, M. A. Khalighi, and S. Bourennane, "Impact of different noise sources on the performance of PIN- and APD-based FSO receivers," *COST IC0802 Workshop, IEEE ConTEL Conference*, pp. 211–218, June 2011, Graz, Austria.

[24] I. S. Gradshteyn and I. M. Ryzhik, *Table of integrals, series, and products*. Academic press, 2014.